

A UNIFORM PRECONDITIONER FOR A NEWTON ALGORITHM FOR TOTAL-VARIATION MINIMIZATION AND MINIMUM-SURFACE PROBLEMS

XUE-CHENG TAI^{*}, RAGNAR WINTHER[†], XIAODI ZHANG[‡], AND WEIYING ZHENG[§]

Abstract. Solution methods for the nonlinear partial differential equation of the Rudin-Osher-Fatemi (ROF) and minimum-surface models are fundamental for many modern applications. Many efficient algorithms have been proposed. First order methods are common. They are popular due to their simplicity and easy implementation. Some second order Newton-type iterative methods have been proposed like Chan-Golub-Mulet method. In this paper, we propose a new Newton-Krylov solver for primal-dual finite element discretization of the ROF model. The method is so simple that we just need to use some diagonal preconditioners during the iterations. Theoretically, the proposed preconditioners are further proved to be robust and optimal with respect to the mesh size, the penalization parameter, the regularization parameter, and the iterative step, essentially it is a parameter independent preconditioner. We first discretize the primal-dual system by using mixed finite element methods, and then linearize the discrete system by Newton's method. Exploiting the well-posedness of the linearized problem on appropriate Sobolev spaces equipped with proper norms, we propose block diagonal preconditioners for the corresponding system solved with the minimum residual method. Numerical results are presented to support the theoretical results.

Key words. ROF model; primal-dual; finite element method; Newton method; block preconditioners

AMS subject classifications. 65M60, 65M12.

1. Introduction. Image restoration is a fundamental and challenging task in image processing. A surge of research has been done in variational and PDE-based approaches. The ROF model due to Rudin, Osher and Fatemi [26] is one of the most successfully and widely used mathematical models. Given an image $f : \Omega \subset \mathbb{R}^d \mapsto \mathbb{R}$, $d = 1, 2, 3$, the ROF model is trying to solve the following minimization problem:

$$\min_v \left\{ E(v) = \int_{\Omega} \alpha |\nabla v| dx + \frac{1}{2} \int_{\Omega} (v - f)^2 dx \right\}, \quad (1.1)$$

where f is the observed image, $\alpha > 0$ is the penalization parameter which controls the trade-off between goodness-of-fit and visibility in its minimizer u . The Euler-Lagrange equation for the minimization problem (1.1) can be formally written as

$$-\alpha \nabla \cdot \left(\frac{\nabla u}{|\nabla u|} \right) + u - f = 0 \quad \text{in } \Omega, \quad \nabla u \cdot \mathbf{n} = 0 \quad \text{on } \partial\Omega. \quad (1.2)$$

Here and after, \mathbf{n} denotes the unit outer normal vector of $\partial\Omega$. This equation indeed characterizes the first-order optimality condition of (1.1), which is also known as the curvature equation [25]. As

^{*}Department of Mathematics, Hong Kong Baptist University, Kowloon Tong Kowloon, Hong Kong. (xuecheng-tai@gmail).

[†]Department of Mathematics, University of Oslo.

[‡]Corresponding Author. Henan Academy of Big Data, Zhengzhou University, Zhengzhou 450052, China. School of Mathematics and Statistics, Zhengzhou University, Zhengzhou 450001, China. (zhangxiaodi@lsec.cc.ac.cn)

[§]LSEC, Academy of Mathematics and Systems Science, Chinese Academy of Sciences, Beijing, 100190, China. School of Mathematical Science, University of Chinese Academy of Sciences, Beijing 100049, China. The fourth author was supported in part by the National Science Fund for Distinguished Young Scholars 11725106 and by China NSF grant 11831016. (zwy@lsec.cc.ac.cn)

a fundamental well studied model in the literature, the ROF model is important for many modern applications include scientific computing, image processing and data sciences.

To deal with the singularity caused by the TV-norm minimization in (1.1), the following regularized minimization problem is often studied,

$$\min_v \left\{ E_\beta(v) = \alpha \int_\Omega \sqrt{|\nabla v|^2 + \beta} dx + \frac{1}{2} \int_\Omega (v - f)^2 dx \right\}, \quad (1.3)$$

where the regularization parameter $\beta > 0$ is typically small. Since the regularized energy functional $E_\beta(v)$ is strictly convex for $\beta > 0$, the minimizer to (1.3) is unique. In [1], it has been shown the solution of the regularized problem (1.3) converges to the solution of (1.1) as $\beta \rightarrow 0$. The convergence has been established rigorously in [35]. It should be noted that this regularization technique is mostly used to compute the minimizer of the total variation energy and its variants [7, 13].

It is well-known that first integral in (1.3) is the surface area of the graph of function v when $\beta = 1$. Thus, model (1.3) is essentially the minimum surface problem when $\beta = 1$. In this work, we will design a fast algorithm which has good convergence properties uniformly with respect to β which means that our algorithm works for the regularized total variation minimization model as well as for the minimum surface model.

The Euler-Lagrange equation corresponds to the minimization problem (1.3) reads

$$-\alpha \nabla \cdot \left(\frac{\nabla u}{\sqrt{|\nabla u|^2 + \beta}} \right) + u - f = 0 \quad \text{in } \Omega, \quad \nabla u \cdot \mathbf{n} = 0 \quad \text{on } \partial\Omega. \quad (1.4)$$

We want to emphasize once more that our proposed method works uniformly with respect to $\beta \in (0, 1]$.

Numerical solution to the minimization problem (1.3) poses a challenging problem due to the presence of a highly nonlinear and non-differentiable term. To get around this difficulty, a large effort has been devoted to construct effective schemes for the minimization problem (1.3) and the PDE problems (1.2) in the past two decades. For instance, the artificial time marching scheme in [24, 26], the lagged diffusivity fixed-point method in [15, 30], Chan-Golub-Mulet method in [12], the Bregman iteration in [16], the augmented Lagrangian technique in [32] and some others in [2, 4, 5, 8, 21, 33]. However, most of these numerical algorithms are gradient-descent type and thus only first-order. Thus, the main motivation of this work is to develop an effective second-order algorithm for the model (1.4).

It is well-known that a “good” algorithm for the nonlinear problem should include not only fast iterative methods but also fast linear solvers for the linear systems obtained after linearization. Solving the linear systems is usually the most important, challenging and time-consuming part in the overall simulation, which is due to the large-scale and ill-conditions of the linear systems. For the underlying nonlinear PDE problem (1.4), the condition number of the linear system tends to infinity when the mesh size is approaching zero. Moreover, the variability of the parameters, such as the penalization parameter α and the regularization parameter β , can additionally influence the scale of the condition number of the system. However, little work has been done to develop robust and efficient solvers for the resulting linear systems. Here, the term “robust” possesses two underlying merits: (i) The convergence rate is independent of the mesh size. (ii) The method is robust with respect to parameters. In order to improve the efficiency of the numerical simulations, we will also focus on designing robust preconditioners for the linearized problem.

Based on the discussion carried out in the previous paragraphs, the purpose of this paper is to propose a preconditioned Newton method for primal-dual finite element discretization of the ROF model. We shall adopt a primal-dual formulation of the model (1.4) which contains the primal variable u , the dual variable \mathbf{p} and the multiplier $\boldsymbol{\lambda}$. We first discretize the primal-dual system by using mixed finite element methods, and then linearize the discrete nonlinear system by Newton's method. Following the operator preconditioning framework in [23], we develop block diagonal preconditioners for the linearized problem. The derivation exploits its well-posedness on appropriate Sobolev spaces equipped with proper norms. We also rigorously prove the condition number of the preconditioned operator is uniformly bounded by a constant independent of the mesh size, the penalization parameter α and the regularization parameter β . Thus, the proposed preconditioners are robust with respect to the mesh size, the smoothing parameter, the regularization parameter, and the iterative step. As a product, we develop a second-order Newton scheme with robust and optimal preconditioners for the model (1.4). Finally, numerical experiments are supplied to test the accuracy of our schemes and validate the uniform robustness of the proposed preconditioners.

We want to emphasize that the essential ideas presented in this work is rather general and can be used for other nonlinear problems. In [18], the harmonic map problem was considered. A uniform preconditioner for the Newton iteration was also constructed using operator preconditioning framework published later in [23]. All these show that the methodology presented here can be used for a large class of problems.

The remainder of the paper is structured as follows. In Section 2, we introduce a primal-dual formulation of the ROF model and present its Newton iterations. Section 3 is devoted to introducing the finite element discretization and giving Newton's linearization for the discrete problem. In Section 4, we derive the well-posedness of the discrete problem on chosen spaces equipped with subtle norms. We propose and analyze the robust preconditioners in Section 5. We carry out several numerical experiments in Section 6 to confirm the efficiency of our proposed algorithms. The paper ends with a concluding remark in Section 7.

2. Our proposed model and Newton algorithm. First we introduce some Sobolev spaces and norms used in this paper. Throughout the paper, we shall denote vector-valued quantities by boldface notations. Let $L^2(\Omega)$ be the usual Hilbert space of square integrable functions which is equipped with the following inner product and norm,

$$\langle u, v \rangle := \int_{\Omega} u(x)v(x)dx, \quad \|u\| := \langle u, u \rangle^{1/2}.$$

Let $H^1(\Omega)$ be its subspace with square integrable gradients, and its standard norm. We also use the space L^∞ with its canonical norm, $\|v\|_\infty = \text{ess sup}_{x \in \Omega} |v(x)|$. For a vector $\mathbf{x} = (x_1, x_2, \dots, x_d) \in \mathbb{R}^d$, we shall use the notation

$$|\mathbf{x}|_\beta = \sqrt{|\mathbf{x}|^2 + \beta} = \sqrt{\sum_{i=1}^d x_i^2 + \beta}.$$

For notation simplicity, we will also use $\langle \cdot, \cdot \rangle$ throughout this work to denote L^2 -type of inner product for vectors, functions include vector functions and duality pairing. From the context where this notation is used, it is clear which inner product or duality this notation is referring to. As usual, ∇ and $\nabla \cdot$ will be used as (distributional) gradient and divergence operators.

Inspired by [32], we introduce the auxiliary variable $\mathbf{p} = \nabla u$ and reformulate (1.3) into an equivalent constrained minimization problem:

$$\min_{\substack{\mathbf{p}, u \\ \mathbf{p} = \nabla u}} \left\{ \int_{\Omega} \alpha |\mathbf{p}|_{\beta} dx + \frac{1}{2} \int_{\Omega} (u - f)^2 dx \right\}. \quad (2.1)$$

The constraint condition can be enforced by use of a Lagrange multiplier $\boldsymbol{\mu}$, and we then seek stationary points to the Lagrangian functional

$$\mathcal{L}(\mathbf{q}, v, \boldsymbol{\mu}) = \int_{\Omega} \left(\alpha |\mathbf{q}|_{\beta} + \frac{1}{2} (v - f)^2 - \boldsymbol{\mu} \cdot (\mathbf{q} - \nabla v) \right) dx.$$

Let $(\mathbf{p}, u, \boldsymbol{\lambda})$ be one saddle point for this problem. As in [20, 22, 28], the first-order optimality condition for (2.1) is:

$$\alpha \mathbf{p} / |\mathbf{p}|_{\beta} - \boldsymbol{\lambda} = 0, \quad u - \nabla \cdot \boldsymbol{\lambda} = f, \quad -\mathbf{p} + \nabla u = 0 \quad \text{in } \Omega, \quad (2.2)$$

in conjunction with the following boundary conditions

$$\boldsymbol{\lambda} \cdot \mathbf{n} = \nabla u \cdot \mathbf{n} = 0 \quad \text{on } \partial\Omega, \quad (2.3)$$

Different from the original Euler-Lagrange equation (1.4) for u , this system contains three variables, i.e. functions u , \mathbf{p} and $\boldsymbol{\lambda}$. Following [12], the method is dubbed as the primal-dual method.

To solve the nonlinear system (2.2)-(2.3), we apply Newton's method as the linearization technique. For convenience, we write this system in the compact form $F(\mathbf{p}, u, \boldsymbol{\lambda}) = 0$, where F is the non-linear map given by

$$F : (\mathbf{p}, u, \boldsymbol{\lambda}) \mapsto (\alpha \mathbf{p} / |\mathbf{p}|_{\beta} - \boldsymbol{\lambda}, u - f - \nabla \cdot \boldsymbol{\lambda}, -\mathbf{p} + \nabla u).$$

Therefore, Newton's method to solve this problem is: Given $(\mathbf{p}^n, u^n, \boldsymbol{\lambda}^n)$, compute $(\mathbf{p}^{n+1}, u^{n+1}, \boldsymbol{\lambda}^{n+1})$ by

$$(\mathbf{p}^{n+1}, u^{n+1}, \boldsymbol{\lambda}^{n+1}) = (\mathbf{p}^n, u^n, \boldsymbol{\lambda}^n) + (\delta \mathbf{p}^n, \delta u^n, \delta \boldsymbol{\lambda}^n), \quad (2.4)$$

where the correction $(\delta \mathbf{p}^n, \delta u^n, \delta \boldsymbol{\lambda}^n)$ is defined by

$$DF(\mathbf{p}^n, u^n, \boldsymbol{\lambda}^n)(\delta \mathbf{p}^n, \delta u^n, \delta \boldsymbol{\lambda}^n) = -F(\mathbf{p}^n, u^n, \boldsymbol{\lambda}^n). \quad (2.5)$$

As usual, $DF(\mathbf{p}^n, u^n, \boldsymbol{\lambda}^n)$ is the Fréchet derivative of the operator F at $(\mathbf{p}^n, u^n, \boldsymbol{\lambda}^n)$. For a given vector field \mathbf{r} , for simplicity, assume that $\mathbf{r}(x) \neq 0$ for all $x \in \Omega$, define the matrix valued function $H(\mathbf{r}) = H(\mathbf{r}(x))$ by

$$H(\mathbf{r}) = \frac{1}{|\mathbf{r}|_{\beta}} \left(\mathbf{I} - \frac{\mathbf{r} \mathbf{r}^t}{|\mathbf{r}|_{\beta}^2} \right).$$

Here \mathbf{r}^t denotes the transpose of \mathbf{r} . It is easy to see that the matrix $H(\mathbf{r})$ is symmetric and satisfies

$$\frac{\beta}{|\mathbf{r}|_{\beta}^3} \leq \frac{H(\mathbf{r}) \boldsymbol{\xi} \cdot \boldsymbol{\xi}}{\boldsymbol{\xi} \cdot \boldsymbol{\xi}} \leq \frac{1}{|\mathbf{r}|_{\beta}}, \quad \forall \boldsymbol{\xi} \in \mathbb{R}^d \setminus \{\mathbf{0}\}. \quad (2.6)$$

In addition, the matrix $H(\mathbf{r})$ is uniformly elliptic provided that $\mathbf{r} \in \mathbf{L}^{\infty}(\Omega)$.

As a consequence, for the n -th step of the Newton iteration the residual system (2.5) can be written as:

$$\begin{cases} \alpha H(\mathbf{p}^n) \delta \mathbf{p}^n - \delta \boldsymbol{\lambda}^n & = \mathbf{r}_{\mathbf{p}}^n, \\ \delta u^n - \nabla \cdot \delta \boldsymbol{\lambda}^n & = r_u^n, \\ -\delta \mathbf{p}^n + \nabla \delta u^n & = \mathbf{r}_{\boldsymbol{\lambda}}^n, \end{cases} \quad (2.7)$$

where the right-hand sides are given by

$$\begin{aligned} \mathbf{r}_{\mathbf{p}}^n &:= -\alpha \mathbf{p}^n / |\mathbf{p}^n|_{\beta} + \boldsymbol{\lambda}^n, \\ r_u^n &:= f - u^n + \nabla \cdot \boldsymbol{\lambda}^n, \\ \mathbf{r}_{\boldsymbol{\lambda}}^n &:= \mathbf{p}^n - \nabla u^n. \end{aligned}$$

In subsequent sections, additional details on the iterations will be provided.

3. Finite element discretization. In this subsection, we introduce the finite element discretization of the system (2.2). Let \mathcal{T}_h be a quasi-uniform and shape-regular simplex mesh of Ω with mesh size h . For any integer $k \geq 0$, $T \in \mathcal{T}_h$, let $P_k(T)$ be the space of polynomials of degree k , and define $\mathbf{P}_k(T) = (P_k(T))^d$. We associate a triple of piecewise polynomial, finite-dimensional spaces to approximate the solution $(\mathbf{p}, u, \boldsymbol{\lambda})$,

$$\begin{aligned} \mathbf{V}_h &:= \{ \mathbf{q} \in \mathbf{L}^2(\Omega) : \mathbf{q}|_T \in \mathbf{P}_0(T), \quad \forall T \in \mathcal{T}_h \}, \\ U_h &:= \{ v \in H^1(\Omega) : v|_T \in P_1(T), \quad \forall T \in \mathcal{T}_h \}, \\ \mathbf{W}_h &:= \{ \boldsymbol{\mu} \in \mathbf{L}^2(\Omega) : \boldsymbol{\mu}|_T \in \mathbf{P}_0(T), \quad \forall T \in \mathcal{T}_h \}. \end{aligned}$$

Based on the above finite element spaces, the finite element approximation of the system (2.2) is formulated as follows: Find $(\mathbf{p}_h, u_h, \boldsymbol{\lambda}_h) \in \mathbf{V}_h \times U_h \times \mathbf{W}_h$ such that for any $(\mathbf{q}_h, v_h, \boldsymbol{\mu}_h) \in \mathbf{V}_h \times U_h \times \mathbf{W}_h$,

$$\begin{cases} \langle \alpha \mathbf{p}_h / |\mathbf{p}_h|_{\beta}, \mathbf{q}_h \rangle - \langle \boldsymbol{\lambda}_h, \mathbf{q}_h \rangle & = 0, \\ \langle u_h, v_h \rangle + \langle \boldsymbol{\lambda}_h, \nabla v_h \rangle & = \langle f, v_h \rangle, \\ -\langle \mathbf{p}_h, \boldsymbol{\mu}_h \rangle + \langle \nabla u_h, \boldsymbol{\mu}_h \rangle & = 0. \end{cases} \quad (3.1)$$

Since we are interested in developing fast solvers for the discrete problem, we do not elaborate on the well-posedness of (3.1) and simply assume that it has a unique solution.

We shall apply the Newton algorithm (2.5) to the above finite element system as well. Let $(\mathbf{p}_h^n, u_h^n, \boldsymbol{\lambda}_h^n) \in \mathbf{V}_h \times U_h \times \mathbf{W}_h$ be the approximate solutions of (3.1) at the n -th Newton iteration. From the linearization in (2.7), for each step of the Newton iteration, the residual equation reads: Find $(\delta \mathbf{p}_h^n, \delta u_h^n, \delta \boldsymbol{\lambda}_h^n) \in \mathbf{V}_h \times U_h \times \mathbf{W}_h$ such that for any $(\mathbf{q}_h, v_h, \boldsymbol{\mu}_h) \in \mathbf{V}_h \times U_h \times \mathbf{W}_h$,

$$\begin{cases} \langle \alpha H(\mathbf{p}_h^n) \delta \mathbf{p}_h^n, \mathbf{q}_h \rangle - \langle \delta \boldsymbol{\lambda}_h^n, \mathbf{q}_h \rangle & = R_{\mathbf{p}}^n(\mathbf{q}_h), \\ \langle \delta u_h^n, v_h \rangle + \langle \delta \boldsymbol{\lambda}_h^n, \nabla v_h \rangle & = R_u^n(v_h), \\ -\langle \delta \mathbf{p}_h^n, \boldsymbol{\mu}_h \rangle + \langle \nabla \delta u_h^n, \boldsymbol{\mu}_h \rangle & = R_{\boldsymbol{\lambda}}^n(\boldsymbol{\mu}_h), \end{cases} \quad (3.2)$$

where the residual functionals are defined by

$$R_{\mathbf{p}}^n(\mathbf{q}_h) := \langle -\alpha \mathbf{p}_h^n / |\mathbf{p}_h^n|_{\beta} + \boldsymbol{\lambda}_h^n, \mathbf{q}_h \rangle,$$

$$\begin{aligned} R_u^n(v_h) &:= \langle f - u_h^n, v_h \rangle - \langle \boldsymbol{\lambda}_h^n, \nabla v_h \rangle, \\ R_\lambda^n(\boldsymbol{\mu}_h) &:= \langle \boldsymbol{p}_h^n - \nabla u_h^n, \boldsymbol{\mu}_h \rangle. \end{aligned}$$

Afterwards, the new solution $(\boldsymbol{p}_h^{n+1}, u_h^{n+1}, \boldsymbol{\lambda}_h^{n+1})$ is given by

$$(\boldsymbol{p}_h^{n+1}, u_h^{n+1}, \boldsymbol{\lambda}_h^{n+1}) = (\boldsymbol{p}_h^n, u_h^n, \boldsymbol{\lambda}_h^n) + (\delta \boldsymbol{p}_h^n, \delta u_h^n, \delta \boldsymbol{\lambda}_h^n). \quad (3.3)$$

Given a $\boldsymbol{r} \in \mathbf{V}_h$, we define the bilinear form $a_{\boldsymbol{r}}(\cdot, \cdot)$ as:

$$\begin{aligned} a_{\boldsymbol{r}}((\boldsymbol{p}_h, u_h, \boldsymbol{\lambda}_h), (\boldsymbol{q}_h, v_h, \boldsymbol{\mu}_h)) &:= \langle \alpha H(\boldsymbol{r}) \boldsymbol{p}_h, \boldsymbol{q}_h \rangle - \langle \boldsymbol{\lambda}_h, \boldsymbol{q}_h \rangle + \langle u_h, v_h \rangle \\ &\quad + \langle \boldsymbol{\lambda}_h, \nabla v_h \rangle - \langle \boldsymbol{p}_h, \boldsymbol{\mu}_h \rangle + \langle \nabla u_h, \boldsymbol{\mu}_h \rangle, \end{aligned}$$

and the residual functional $\ell_h(\cdot)$ as:

$$\ell(\boldsymbol{q}_h, v_h, \boldsymbol{\mu}_h) := R_{\boldsymbol{p}}^n(\boldsymbol{q}_h) + R_u^n(v_h) + R_\lambda^n(\boldsymbol{\mu}_h).$$

Write $X_h := \mathbf{V}_h \times U_h \times \mathbf{W}_h$, then the problem (3.2) can be equivalently written as: Given $(\boldsymbol{p}_h^n, u_h^n, \boldsymbol{\lambda}_h^n) \in X_h$, find $(\delta \boldsymbol{p}_h^n, \delta u_h^n, \delta \boldsymbol{\lambda}_h^n) \in X_h$ such that

$$a_{\boldsymbol{p}_h^n}((\delta \boldsymbol{p}_h^n, \delta u_h^n, \delta \boldsymbol{\lambda}_h^n), (\boldsymbol{q}_h, v_h, \boldsymbol{\mu}_h)) = \ell(\boldsymbol{q}_h, v_h, \boldsymbol{\mu}_h), \quad \forall (\boldsymbol{q}_h, v_h, \boldsymbol{\mu}_h) \in X_h. \quad (3.4)$$

For a given $\boldsymbol{r} \in \mathbf{V}_h$, we introduce the operator $\mathcal{A}_h(\boldsymbol{r}) : X_h \rightarrow X_h^*$ defined by

$$\langle \mathcal{A}_h(\boldsymbol{r})(\boldsymbol{p}_h, u_h, \boldsymbol{\lambda}_h), (\boldsymbol{q}_h, v_h, \boldsymbol{\mu}_h) \rangle := a_{\boldsymbol{r}}((\boldsymbol{p}_h, u_h, \boldsymbol{\lambda}_h), (\boldsymbol{q}_h, v_h, \boldsymbol{\mu}_h)), \quad \forall (\boldsymbol{p}_h, u_h, \boldsymbol{\lambda}_h), (\boldsymbol{q}_h, v_h, \boldsymbol{\mu}_h) \in X_h. \quad (3.5)$$

We remind that $\langle \cdot, \cdot \rangle$ here refers to the duality pairing between X_h^* and X_h . Roughly speaking, $\mathcal{A}_h(\boldsymbol{r})$ is the discrete version of the following operator,

$$\mathcal{A}(\boldsymbol{r}) := \begin{pmatrix} \alpha H(\boldsymbol{r}) & 0 & -\mathbf{I} \\ 0 & \mathbf{I} & -\nabla \cdot \\ -\mathbf{I} & \nabla & 0 \end{pmatrix}. \quad (3.6)$$

We first note the form $\langle \mathcal{A}_h(\boldsymbol{r}) \cdot, \cdot \rangle$ is symmetric, reflecting the symmetry of the saddle point operator $\mathcal{A}_h(\boldsymbol{r})$. Besides that, for the n -th step of the Newton iteration, we need to solve a linear system with the operator $\mathcal{A}_h(\boldsymbol{p}_h^n)$ as the coefficient matrix. Since the operator $\mathcal{A}_h(\boldsymbol{r})$ is indefinite and symmetric, we solve the linear system by the minimum residual method (MINRES) [23]. However, as one of the Krylov space methods, the convergence rate of MINRES depends on the condition number and the spectrum of $\mathcal{A}_h(\boldsymbol{r})$. This motivates the study of efficient preconditioners for the operator $\mathcal{A}_h(\boldsymbol{r})$.

REMARK 3.1. *Using the inverse estimate in the finite element space \mathbf{V}_h , we have*

$$\|\boldsymbol{p}_h\|_\infty \leq C_h \|\boldsymbol{p}_h\|, \quad (3.7)$$

where the embedding constant C_h depends on the mesh size but is finite. Thus, $H(\boldsymbol{p}_h^n) \in \mathbf{L}^\infty(\Omega)$ is uniformly elliptic, c.f (2.6). Accordingly, problems (3.1) and (3.2) are well-defined.

4. Well-posedness of the linear system for the Newton algorithm . Now we discuss the well-posedness of scheme (3.4), which is the foundation of the preconditioners we proposed. For this end, we will use Babuška-Brezzi theory to analyze the mapping properties of the operator $\mathcal{A}_h(\mathbf{r})$ for any $\mathbf{r} \in \mathbf{V}_h$.

As discussed in [23], ensuring that the continuity constants and the inf-sup constants are independent of the physical parameters and the discretized parameters is crucial to design robust block preconditioners for solving our problem. Note that the natural bound on the saddle point operator $\mathcal{A}_h(\mathbf{r})$ depends on the vector field \mathbf{r} . Therefore, we equip the space X_h with the following \mathbf{r} -dependent inner-product

$$((\mathbf{p}_h, u_h, \boldsymbol{\lambda}_h), (\mathbf{q}_h, v_h, \boldsymbol{\mu}_h))_{X_r} := \alpha \langle H(\mathbf{r})\mathbf{p}_h, \mathbf{q}_h \rangle + \langle u_h, v_h \rangle + \alpha \langle H(\mathbf{r})\nabla u_h, \nabla v_h \rangle + \alpha^{-1} \langle H(\mathbf{r})^{-1}\boldsymbol{\lambda}_h, \boldsymbol{\mu}_h \rangle, \quad (4.1)$$

and norm

$$\|(\mathbf{q}_h, v_h, \boldsymbol{\mu}_h)\|_{X_r}^2 := \alpha \langle H(\mathbf{r})\mathbf{q}_h, \mathbf{q}_h \rangle + \|v_h\|^2 + \alpha \langle H(\mathbf{r})\nabla v_h, \nabla v_h \rangle + \alpha^{-1} \langle H(\mathbf{r})^{-1}\boldsymbol{\mu}_h, \boldsymbol{\mu}_h \rangle. \quad (4.2)$$

It is clear that the corresponding norm for the dual space X_h^* depends on \mathbf{r} and α . Thanks to the estimate (3.7) and (2.6), the matrix $H(\mathbf{r})$ is uniformly elliptic and invertible. Hence, the weighted norm (4.2) is well-defined in X_h .

After the introduction of these notations, we are able to show that the operator $\mathcal{A}_h(\mathbf{r})$ has the following properties.

LEMMA 4.1 (Boundedness of $\mathcal{A}_h(\mathbf{r})$). *There is a positive constant c_0 , independent of $\mathbf{r}, \alpha, \beta$ and h , such that for all $(\mathbf{p}_h, u_h, \boldsymbol{\lambda}_h), (\mathbf{q}_h, v_h, \boldsymbol{\mu}_h) \in X_h$, we have*

$$\langle \mathcal{A}_h(\mathbf{r})(\mathbf{p}_h, u_h, \boldsymbol{\lambda}_h), (\mathbf{q}_h, v_h, \boldsymbol{\mu}_h) \rangle \leq c_0 \|(\mathbf{p}_h, u_h, \boldsymbol{\lambda}_h)\|_{X_r} \|(\mathbf{q}_h, v_h, \boldsymbol{\mu}_h)\|_{X_r}.$$

Proof. This follows directly from the definition of the operator $\mathcal{A}_h(\mathbf{r})$ and the definition of $\|\cdot\|_{X_r}$ with $c_0 = 2$. \square

We define the associated kernel space $Z_h \subset \mathbf{V}_h \times U_h$ by

$$Z_h = \{(\mathbf{p}_h, u_h) \in \mathbf{V}_h \times U_h \mid \langle \nabla u_h - \mathbf{p}_h, \boldsymbol{\mu}_h \rangle = 0, \quad \forall \boldsymbol{\mu}_h \in \mathbf{W}_h\}.$$

Note that $\nabla u_h \in \mathbf{W}_h$ and $\mathbf{p}_h \in \mathbf{W}_h$, thus taking $\boldsymbol{\mu}_h = \nabla u_h - \mathbf{p}_h$ gives $\mathbf{p}_h = \nabla u_h$. Consequently, the discrete kernel space Z_h is further portrayed as

$$Z_h = \{(\mathbf{p}_h, u_h) \in \mathbf{V}_h \times U_h \mid \mathbf{p}_h = \nabla u_h\}.$$

LEMMA 4.2 (Coercivity on the kernel space). *There is a positive constant c_1 , independent of $\mathbf{r}, \alpha, \beta$ and h , such that for all $(\mathbf{p}_h, u_h) \in Z_h$, we have*

$$\langle \mathcal{A}_h(\mathbf{r})(\mathbf{p}_h, u_h, 0), (\mathbf{p}_h, u_h, 0) \rangle \geq c_1 \|(\mathbf{p}_h, u_h, 0)\|_{X_r}^2.$$

Proof. Just observe that on Z_h

$$\langle \mathcal{A}_h(\mathbf{r})(\mathbf{p}_h, u_h, 0), (\mathbf{p}_h, u_h, 0) \rangle = \langle \alpha H(\mathbf{r})\mathbf{p}_h, \mathbf{p}_h \rangle + \|u_h\|^2$$

$$= \frac{1}{2} \langle \alpha H(\mathbf{r}) \mathbf{p}_h, \mathbf{p}_h \rangle + \|u_h\|^2 + \frac{1}{2} \langle \alpha H(\mathbf{r}) \nabla u_h, \nabla u_h \rangle,$$

and that

$$\|(\mathbf{p}_h, u_h, 0)\|_{X_r}^2 = \langle \alpha H(\mathbf{r}) \mathbf{p}_h, \mathbf{p}_h \rangle + \|u_h\|^2 + \alpha \langle H(\mathbf{r}) \nabla u_h, \nabla u_h \rangle.$$

Then the desired inequality holds with $c_1 = 1/2$. \square

LEMMA 4.3 (Inf-sup condition). *There is a positive constant c_2 , independent of $\mathbf{r}, \alpha, \beta$ and h , such that*

$$\sup_{(\mathbf{q}_h, v_h) \in \mathbf{V}_h \times U_h} \frac{\langle \mathcal{A}_h(\mathbf{r})(0, 0, \boldsymbol{\lambda}_h), (\mathbf{q}_h, v_h, 0) \rangle}{\|(\mathbf{q}_h, v_h, 0)\|_{X_r}} \geq c_2 \|(0, 0, \boldsymbol{\lambda}_h)\|_{X_r}, \quad \forall \boldsymbol{\lambda} \in \mathbf{W}_h.$$

Proof. We have that

$$\begin{aligned} \sup_{(\mathbf{q}_h, v_h) \in \mathbf{V}_h \times U_h} \frac{\langle \mathcal{A}_h(\mathbf{r})(0, 0, \boldsymbol{\lambda}_h), (\mathbf{q}_h, v_h, 0) \rangle}{\|(\mathbf{q}_h, v_h, 0)\|_{X_r}} &\geq \sup_{(\mathbf{q}_h, 0) \in \mathbf{V}_h \times U_h} \frac{-\langle \boldsymbol{\lambda}_h, \mathbf{q}_h \rangle}{(\alpha \langle H(\mathbf{r}) \mathbf{q}_h, \mathbf{q}_h \rangle)^{1/2}} \\ &\geq (\alpha^{-1} \langle H(\mathbf{r})^{-1} \boldsymbol{\lambda}_h, \boldsymbol{\lambda}_h \rangle)^{1/2}, \end{aligned}$$

where the last inequality follows by taking $\mathbf{q}_h = -\alpha^{-1} H(\mathbf{r})^{-1} \boldsymbol{\lambda}_h$. Since

$$\|(0, 0, \boldsymbol{\lambda}_h)\|_{X_r} = (\alpha^{-1} \langle H(\mathbf{r})^{-1} \boldsymbol{\lambda}_h, \boldsymbol{\lambda}_h \rangle)^{1/2}.$$

This shows that the desired inequality holds with $c_2 = 1$. \square

With the three lemmas above, we obtain the main result of this section.

THEOREM 4.1. *At each iteration for the Newton updating, the discretized problem (3.2) is well-posed.*

Proof. By similar arguments of Theorem 5.2 in [23], it is straight-forward to reach the conclusion.

\square

Using adequately weighted spaces, we have that $\mathcal{A}_h(\mathbf{r})$ is an isomorphism from X_h to X_h^* such that $\|\mathcal{A}_h(\mathbf{r})\|_{\mathcal{L}(X_h, X_h^*)}$ and $\|(\mathcal{A}_h(\mathbf{r}))^{-1}\|_{\mathcal{L}(X_h^*, X_h)}$ are bounded independently of mesh sizes and the parameters. That is

$$\|\mathcal{A}_h(\mathbf{r})\|_{\mathcal{L}(X_h, X_h^*)} \leq C, \quad \|(\mathcal{A}_h(\mathbf{r}))^{-1}\|_{\mathcal{L}(X_h^*, X_h)} \leq c^{-1}, \quad (4.3)$$

where the constants C and c only depend on c_0, c_1, c_2 .

5. Robust preconditioners. In this section, we develop and analyze robust preconditioners. Let $\mathcal{B}_h(\mathbf{r})$ be the "Riesz-operator" mapping from X_h^* to X_h , which is induced by the weighted norm $\|\cdot\|_{X_r}$, for given $(\mathbf{p}_h, u_h, \boldsymbol{\lambda}_h) \in X_h^*$:

$$(\mathcal{B}_h(\mathbf{r})(\mathbf{p}_h, u_h, \boldsymbol{\lambda}_h), (\mathbf{q}_h, v_h, \boldsymbol{\mu}_h))_{X_r} := \langle (\mathbf{p}_h, u_h, \boldsymbol{\lambda}_h), (\mathbf{q}_h, v_h, \boldsymbol{\mu}_h) \rangle, \quad (\mathbf{q}_h, v_h, \boldsymbol{\mu}_h) \in X_h.$$

By using (4.1) and (4.2), we can see that it takes the following explicit form,

$$\mathcal{B}_h(\mathbf{r}) = \begin{pmatrix} \alpha H(\mathbf{r}) & 0 & 0 \\ 0 & S_{r,h} & 0 \\ 0 & 0 & \alpha^{-1} H(\mathbf{r})^{-1} \end{pmatrix}^{-1}, \quad (5.1)$$

where the operator $S_{\mathbf{r},h}: V_h \mapsto V_h^*$ is defined by

$$\langle S_{\mathbf{r},h}u_h, v_h \rangle := \langle u_h, v_h \rangle + \langle \alpha H(\mathbf{r})\nabla u_h, \nabla v_h \rangle, \quad \forall u_h, v_h \in V_h.$$

In fact, $S_{\mathbf{r},h}$ is the finite element discretization for the operator $I - \nabla \cdot (H(\mathbf{r})\nabla)$ with Neumann boundary conditions. Note that the matrix $H(\mathbf{r})$ is symmetric and uniformly elliptic, the second block, $S_{\mathbf{r},h}$, is invertible. Following the operator preconditioning framework [23], the operator $\mathcal{B}_h(\mathbf{r})$ is proposed as the preconditioner for $\mathcal{A}_h(\mathbf{r})$.

In the following we estimate the condition number of the preconditioned operator $\mathcal{B}_h(\mathbf{r})\mathcal{A}_h(\mathbf{r})$ using the following formula:

$$\kappa(\mathcal{B}_h(\mathbf{r})\mathcal{A}_h(\mathbf{r})) = \|\mathcal{B}_h(\mathbf{r})\mathcal{A}_h(\mathbf{r})\|_{\mathcal{L}(X_h, X_h)} \left\| (\mathcal{B}_h(\mathbf{r})\mathcal{A}_h(\mathbf{r}))^{-1} \right\|_{\mathcal{L}(X_h, X_h)}. \quad (5.2)$$

THEOREM 5.1. *The condition number $\kappa(\mathcal{B}_h(\mathbf{r})\mathcal{A}_h(\mathbf{r}))$ has a uniform bound, independent of \mathbf{r} , α , β and h , in the sense that*

$$1 \leq \kappa(\mathcal{B}_h(\mathbf{r})\mathcal{A}_h(\mathbf{r})) \leq C/c,$$

where C and c are defined by (4.3).

Proof. We note that the operator $\mathcal{B}_h(\mathbf{r})$ has the property that

$$\|\mathcal{B}_h(\mathbf{r})\|_{\mathcal{L}(X_h^*, X_h)} = \left\| (\mathcal{B}_h(\mathbf{r}))^{-1} \right\|_{\mathcal{L}(X_h, X_h^*)} = 1.$$

Then we have

$$\|\mathcal{B}_h(\mathbf{r})\mathcal{A}_h(\mathbf{r})\|_{\mathcal{L}(X_h, X_h)} = \|\mathcal{A}_h(\mathbf{r})\|_{\mathcal{L}(X_h, X_h^*)} \leq C,$$

and

$$\left\| (\mathcal{B}_h(\mathbf{r})\mathcal{A}_h(\mathbf{r}))^{-1} \right\|_{\mathcal{L}(X_h, X_h)} \leq \left\| (\mathcal{A}_h(\mathbf{r}))^{-1} \right\|_{\mathcal{L}(X_h^*, X_h)} \left\| (\mathcal{B}_h(\mathbf{r}))^{-1} \right\|_{\mathcal{L}(X_h, X_h^*)} \leq c^{-1}.$$

We get the desired result using (5.2). \square

This theorem suggests that $\mathcal{B}_h(\mathbf{r})$ is a “good” preconditioner for $\mathcal{A}_h(\mathbf{r})$ in the sense that the preconditioned operator has a condition number which is independent of the mesh size (h), the penalization parameter (α), the regularization parameter (β) and the iterative step (n). We are using MINRES to solve the preconditioned linear system at each Newton iteration. We have the following convergence result for the MINRES.

THEOREM 5.2. *If x^0 is the the initial value, x^m is the m -th iteration of MINRES method and x is the exact solution, then there exists a constant $\delta \in (0, 1)$, only depending on the condition number $\kappa(\mathcal{B}_h(\mathbf{r})\mathcal{A}_h(\mathbf{r}))$, such that*

$$\langle \mathcal{B}_h(\mathbf{r})\mathcal{A}_h(\mathbf{r})(x - x^m), \mathcal{A}_h(\mathbf{r})(x - x^m) \rangle^{\frac{1}{2}} \leq 2\delta^m \langle \mathcal{B}_h(\mathbf{r})\mathcal{A}_h(\mathbf{r})(x - x^0), \mathcal{A}_h(\mathbf{r})(x - x^0) \rangle^{\frac{1}{2}}.$$

Moreover, an estimate leads to

$$\delta = \frac{\kappa(\mathcal{B}_h(\mathbf{r})\mathcal{A}_h(\mathbf{r})) - 1}{\kappa(\mathcal{B}_h(\mathbf{r})\mathcal{A}_h(\mathbf{r})) + 1} \leq \frac{C - c}{C + c}.$$

Proof. Since the operator $\mathcal{B}_h(\mathbf{r}) \in \mathcal{L}(X_h^*, X_h)$ is symmetric and positive definite, $\langle (\mathcal{B}_h(\mathbf{r}))^{-1} \cdot, \cdot \rangle$ defines an inner product on X_h . Furthermore, it is easy to see that the preconditioned operator $\mathcal{B}_h(\mathbf{r})\mathcal{A}_h(\mathbf{r}) \in \mathcal{L}(X_h, X_h)$ is symmetric in this inner product. So we shall use MINRES method which is defined with respect to the inner product $\langle (\mathcal{B}_h(\mathbf{r}))^{-1} \cdot, \cdot \rangle$. The estimate is obtained by applying Theorem 2.2 in [23]. \square

The inverse of $S_{\mathbf{r},h}$ needs to solve an elliptic linear problem. It could be costly to solve this elliptic problem, especially for three dimensional problems: Thus, we consider the following inexact preconditioner

$$\tilde{\mathcal{B}}_h(\mathbf{r}) = \begin{pmatrix} \alpha H(\mathbf{r}) & 0 & 0 \\ 0 & \tilde{S}_{\mathbf{r},h}^{-1} & 0 \\ 0 & 0 & \alpha^{-1} H(\mathbf{r})^{-1} \end{pmatrix}^{-1}. \quad (5.3)$$

Here, $\tilde{S}_{\mathbf{r},h}$ is an operator that is spectrally equivalent to the action of the inverse of the block $S_{\mathbf{r},h}$ in the following sense:

$$c_{1,s} \langle S_{\mathbf{r},h}^{-1} v_h, v_h \rangle \leq \langle \tilde{S}_{\mathbf{r},h} v_h, v_h \rangle \leq c_{2,s} \langle S_{\mathbf{r},h}^{-1} v_h, v_h \rangle \quad \forall v_h \in V_h, \quad (5.4)$$

where the constants $c_{1,s}$ and $c_{2,s}$ are independent of the mesh size, the penalization parameter, the regularization parameter and the iterative step. In the implementation, $\tilde{S}_{\mathbf{r},h}$ is obtained by using standard multigrid method, algebraic multigrid method (AMG) or domain decomposition method. Based on the results in [6, 17, 34], we think the estimate (5.4) will hold if we use AMG to produce $\tilde{S}_{\mathbf{r},h}$, and our experiments seem to confirm this. Thus, the proposed preconditioner is very cheap and easy-to-implement.

When using $\tilde{\mathcal{B}}_h(\mathbf{r})$ as the preconditioner, we have the following results regarding the convergence estimate of the corresponding preconditioned MINRES method.

THEOREM 5.3. *Assume that (5.4) is satisfied, then we have*

$$1 \leq \kappa \left(\tilde{\mathcal{B}}_h(\mathbf{r})\mathcal{A}_h(\mathbf{r}) \right) \leq \frac{C\hat{c}_2}{c\hat{c}_1},$$

where $\hat{c}_1 = \min(c_{1,s}, 1)$ and $\hat{c}_2 = \max(c_{2,s}, 1)$. Moreover, if x^0 is the initial value, x^m is the m -th iteration of MINRES method and x is the exact solution, then there exists a constant $\delta \in (0, 1)$, only depending on the condition number $\kappa \left(\tilde{\mathcal{B}}_h(\mathbf{r})\mathcal{A}_h(\mathbf{r}) \right)$, such that

$$\left\langle \tilde{\mathcal{B}}_h(\mathbf{r})\mathcal{A}_h(\mathbf{r}) (x - x^m), \mathcal{A}_h(\mathbf{r}) (x - x^m) \right\rangle^{\frac{1}{2}} \leq 2\delta^m \left\langle \tilde{\mathcal{B}}_h(\mathbf{r})\mathcal{A}_h(\mathbf{r}) (x - x^0), \mathcal{A}_h(\mathbf{r}) (x - x^0) \right\rangle^{\frac{1}{2}}.$$

Furthermore, an estimate leads to

$$\delta = \frac{\kappa \left(\tilde{\mathcal{B}}_h(\mathbf{r})\mathcal{A}_h(\mathbf{r}) \right) - 1}{\kappa \left(\tilde{\mathcal{B}}_h(\mathbf{r})\mathcal{A}_h(\mathbf{r}) \right) + 1} \leq \frac{\hat{c}_2 C - \hat{c}_1 c}{\hat{c}_2 C + \hat{c}_1 c}.$$

Proof. We only need to estimate the condition number of the preconditioned operator $\tilde{\mathcal{B}}_h(\mathbf{r})\mathcal{A}_h(\mathbf{r})$, the result of the convergence of preconditioned MINRES method is obvious. From (5.4), we can see that $\tilde{\mathcal{B}}_h(\mathbf{r})$ satisfies

$$\hat{c}_1(x, x)_{\mathcal{B}_h(\mathbf{r})} \leq (x, x)_{\tilde{\mathcal{B}}_h(\mathbf{r})} \leq \hat{c}_2(x, x)_{\mathcal{B}_h(\mathbf{r})}. \quad (5.5)$$

This implies that

$$\left\| \tilde{\mathcal{B}}_h(\mathbf{r}) (\mathcal{B}_h(\mathbf{r}))^{-1} \right\|_{\mathcal{L}(X_h, X_h)} \leq \hat{c}_2, \quad \left\| \left(\tilde{\mathcal{B}}_h(\mathbf{r}) (\mathcal{B}_h(\mathbf{r}))^{-1} \right)^{-1} \right\|_{\mathcal{L}(X_h, X_h)} \leq \hat{c}_1^{-1}.$$

Similar to the proof of Theorem 5.1, we have

$$\begin{aligned} \left\| \tilde{\mathcal{B}}_h(\mathbf{r})\mathcal{A}_h(\mathbf{r}) \right\|_{\mathcal{L}(X_h, X_h)} &= \left\| \tilde{\mathcal{B}}_h(\mathbf{r}) (\mathcal{B}_h(\mathbf{r}))^{-1} \mathcal{B}_h(\mathbf{r})\mathcal{A}_h(\mathbf{r}) \right\|_{\mathcal{L}(X_h, X_h)} \\ &\leq \left\| \tilde{\mathcal{B}}_h(\mathbf{r}) (\mathcal{B}_h(\mathbf{r}))^{-1} \right\|_{\mathcal{L}(X_h, X_h)} \left\| \mathcal{B}_h(\mathbf{r})\mathcal{A}_h(\mathbf{r}) \right\|_{\mathcal{L}(X_h, X_h)} \leq C\hat{c}_2, \end{aligned}$$

and

$$\begin{aligned} \left\| \left(\tilde{\mathcal{B}}_h(\mathbf{r})\mathcal{A}_h(\mathbf{r}) \right)^{-1} \right\|_{\mathcal{L}(X_h, X_h)} &= \left\| \left(\tilde{\mathcal{B}}_h(\mathbf{r}) (\mathcal{B}_h(\mathbf{r}))^{-1} \mathcal{B}_h(\mathbf{r})\mathcal{A}_h(\mathbf{r}) \right)^{-1} \right\|_{\mathcal{L}(X_h, X_h)} \\ &\leq \left\| (\mathcal{B}_h(\mathbf{r})\mathcal{A}_h(\mathbf{r}))^{-1} \right\|_{\mathcal{L}(X_h, X_h)} \left\| \left(\tilde{\mathcal{B}}_h(\mathbf{r}) (\mathcal{B}_h(\mathbf{r}))^{-1} \right)^{-1} \right\|_{\mathcal{L}(X_h, X_h)} \leq c^{-1}\hat{c}_1^{-1}. \end{aligned}$$

Therefore, we get the estimate of the condition number. \square

As a consequence, the exact methods for the block solvers in the preconditioner $\mathcal{B}_h(\mathbf{r})$ can be replaced by inexact methods and still maintain the desired properties. So far, we have gotten a robust and effective solver when solving the linearized systems. This makes it very cheap to solve the system for each iteration for Newton updating. Together, it yields a second-order Newton scheme with robust and optimal preconditioners.

6. Numerical experiments. In this section, we present some numerical experiments to verify the convergence rate of the finite element approximation to our model, and to demonstrate the robustness of the preconditioners. A set of two-dimensional examples are reported below. All codes were written in MATLAB based on the open-source finite element library *iFEM* [14].

For comparison, we also implement the following fixed point method, which is also known as Picard method. For this method, given the n -th iteration $(\mathbf{p}_h^n, u_h^n, \boldsymbol{\lambda}_h^n) \in \mathbf{V}_h \times U_h \times \mathbf{W}_h$, $(\mathbf{p}_h^{n+1}, u_h^{n+1}, \boldsymbol{\lambda}_h^{n+1}) \in \mathbf{V}_h \times U_h \times \mathbf{W}_h$ is solved by

$$\begin{cases} \langle \alpha \mathbf{p}_h^{n+1} / |\mathbf{p}_h^n|_\beta, \mathbf{q}_h \rangle - \langle \boldsymbol{\lambda}_h^{n+1}, \mathbf{q}_h \rangle &= 0 \quad \forall \mathbf{q}_h \in \mathbf{V}_h, \\ \langle u_h^{n+1}, v_h \rangle + \langle \boldsymbol{\lambda}_h^{n+1}, \nabla v_h \rangle - \langle f, v_h \rangle &= 0 \quad \forall v_h \in U_h, \\ -\langle \mathbf{p}_h^{n+1}, \boldsymbol{\mu}_h \rangle + \langle \nabla u_h^{n+1}, \boldsymbol{\mu}_h \rangle &= 0 \quad \forall \boldsymbol{\mu}_h \in \mathbf{W}_h. \end{cases} \quad (6.1)$$

With the notation in Section 3, its residual form reads: Find $(\delta \mathbf{p}_h^n, \delta u_h^n, \delta \boldsymbol{\lambda}_h^n) \in \mathbf{V}_h \times U_h \times \mathbf{W}_h$ such that for any $(\mathbf{q}_h, v_h, \boldsymbol{\mu}_h) \in \mathbf{V}_h \times U_h \times \mathbf{W}_h$,

$$\begin{cases} \langle \alpha \hat{H}(\mathbf{p}_h^n) \delta \mathbf{p}_h^n, \mathbf{q}_h \rangle - \langle \delta \boldsymbol{\lambda}_h^n, \mathbf{q}_h \rangle &= R_p^n(\mathbf{q}_h), \\ \langle \delta u_h^n, v_h \rangle + \langle \delta \boldsymbol{\lambda}_h^n, \nabla v_h \rangle &= R_u^n(v_h), \\ -\langle \delta \mathbf{p}_h^n, \boldsymbol{\mu}_h \rangle + \langle \nabla \delta u_h^n, \boldsymbol{\mu}_h \rangle &= R_\lambda^n(\boldsymbol{\mu}_h), \end{cases} \quad (6.2)$$

where $\widehat{H}(\mathbf{p}_h^n) := 1/|\mathbf{p}_h^n|_\beta$. Thus, the new solution $(\mathbf{p}_h^{n+1}, u_h^{n+1}, \boldsymbol{\lambda}_h^{n+1})$ is given by

$$(\mathbf{p}_h^{n+1}, u_h^{n+1}, \boldsymbol{\lambda}_h^{n+1}) = (\mathbf{p}_h^n, u_h^n, \boldsymbol{\lambda}_h^n) + (\delta\mathbf{p}_h^n, \delta u_h^n, \delta\boldsymbol{\lambda}_h^n). \quad (6.3)$$

Clearly, the difference of Newton method and Picard method lies on the matrix $H(\mathbf{r})$ and the scalar $\widehat{H}(\mathbf{r})$. Note that $\widehat{H}(\mathbf{r})$ is bounded above by $1/\beta$ and below by zero. Hence, the theory for Newton method in Sections 4-5 also applies to the Picard method as long as we replace $H(\mathbf{r})$ by $\widehat{H}(\mathbf{r})$ in $\mathcal{A}_h(\mathbf{r})$, $\mathcal{B}_h(\mathbf{r})$ and $\widetilde{\mathcal{B}}_h(\mathbf{r})$. For convenience, we still use the notation $\mathcal{A}_h(\mathbf{r})$, $\mathcal{B}_h(\mathbf{r})$ and $\widetilde{\mathcal{B}}_h(\mathbf{r})$ for Picard method. From (3.2), (6.2), (5.1) and (5.3), we know that the costs of per iteration for Picard method and Newton method are almost the same. Thus, for convenience, only the iteration numbers needed by both methods are used for comparison in this section.

6.1. Implementation of block preconditioners. First of all, we discuss some implementation details of the proposed block preconditioners. To solve the linear system obtained from the finite element discretization, we use the MINRES method as an outer iterative solver, with the tolerance for the relative residual in the energy norm set to $\varepsilon = 10^{-10}$. The block preconditioners designed in Section 5 are used to accelerate the convergence rate of MINRES. In the following, we implement both exact and inexact inner solvers, $\mathcal{B}_h(\mathbf{r})$ and $\widetilde{\mathcal{B}}_h(\mathbf{r})$. As we know, inverting the proposed block preconditioners ends up with inverting diagonal blocks. Therefore, the main difference in implementation is how to invert the second diagonal block. For the exact preconditioner $\mathcal{B}_h(\mathbf{r})$, we call direct solvers implemented in MATLAB. While for the inexact preconditioner $\widetilde{\mathcal{B}}_h(\mathbf{r})$, we mainly call AMG preconditioned conjugate gradient (PCG) method to define the operator $\widetilde{S}_{r,h}$. The tolerance of PCG in terms of l_2 -norm of the relative residual is $\varepsilon_0 = 10^{-3}$. The AMG we used is the classical algebraic multigrid method with Ruge-Stuben coarsening and standard interpolation [14, 34].

Without specifications, the initial guess $(\mathbf{p}_h^0, u_h^0, \boldsymbol{\lambda}_h^0)$ is taken to be the zero solution and the relative tolerances are set by 10^{-6} for the nonlinear iteration. Here the maximal iteration number of the MINRES solver is set by $N = 200$. For the sake of convenience, we denote N_{Newton} by the number of Newton's iterations, N_{Picard} by the number of Picard's iterations and N_{MINRES} by the average number of preconditioned MINRES iterations for solving the linearized problem.

To ensure the global convergence of the Newton algorithm, we introduce an additional damping parameter θ . Let \mathbf{b}^n be the vector representation of the right hand of (3.4) at n -th iteration, we use the classical backtracking line search method, which selects as step length θ^n to be the first number in the sequence of $\{1/2^k\}_{k=0}^\infty$ that satisfies the following criterion

$$\left\| \mathbf{b}^{k+1} \right\|_{l_2} \leq (1 - \sigma\theta_k) \left\| \mathbf{b}^n \right\|_{l_2},$$

where σ is chosen as 10^{-4} . Thus, the damped Newton-updating is given by

$$(\mathbf{p}_h^{n+1}, u_h^{n+1}, \boldsymbol{\lambda}_h^{n+1}) = (\mathbf{p}_h^n, u_h^n, \boldsymbol{\lambda}_h^n) + \theta^n (\delta\mathbf{p}_h^n, \delta u_h^n, \delta\boldsymbol{\lambda}_h^n). \quad (6.4)$$

6.2. Numerical results. This subsection is to report on some numerical experiments.

EXAMPLE 6.1. *This example is to test the convergence rate of finite element solutions and the robustness of the preconditioners for some smooth problems. The computational domain Ω is set as $(0, 1)^2$. The function f is chosen so that the exact solutions are given by*

$$u = \cos(\pi x) \cos(\pi y),$$

TABLE 6.1
The mesh sizes and the numbers of DOFs.

Mesh	h	DOFs for \mathbf{p}_h	DOFs for u_h	DOFs for $\boldsymbol{\lambda}_h$	Total DOFs
\mathcal{T}_1	6.25e-02	1,024	289	1,024	2,337
\mathcal{T}_2	3.13e-02	4,096	1,089	4,096	9,281
\mathcal{T}_3	1.56e-02	16,384	4,225	16,384	36,993
\mathcal{T}_4	7.81e-03	65,536	16,641	65,536	147,713

TABLE 6.2
Errors and convergence rates for $(\mathbf{p}_h, u_h, \boldsymbol{\lambda}_h)$ (Example 6.1).

h	$\ \mathbf{p} - \mathbf{p}_h\ _0$	Order	$\ \boldsymbol{\lambda} - \boldsymbol{\lambda}_h\ _0$	Order
6.25e-02	2.17585e-01	—	8.95410e-02	—
3.13e-02	1.08967e-01	1.00	4.52978e-02	0.98
1.56e-02	5.45105e-02	1.00	2.27351e-02	1.00
7.81e-03	2.72596e-02	1.00	1.13809e-02	1.00

h	$\ u - u_h\ _1$	Order	$\ u - u_h\ _0$	Order
6.25e-02	2.17595e-01	—	7.97886e-03	—
3.13e-02	1.08968e-01	1.00	2.02665e-03	1.98
1.56e-02	5.45107e-02	1.00	5.12786e-04	1.98
7.81e-03	2.72596e-02	1.00	1.32618e-04	1.95

$$\mathbf{p} = -\pi (\sin(\pi x) \cos(\pi y), \cos(\pi x) \sin(\pi y))^\top,$$

$$\boldsymbol{\lambda} = -\frac{\pi\alpha}{|\mathbf{p}|_\beta} (\sin(\pi x) \cos(\pi y), \cos(\pi x) \sin(\pi y))^\top.$$

We first carry out the numerical experiment with $\alpha = \beta = 1$. Table 6.1 shows the information for the meshes and the number of degrees of freedom which we are using. Based on the results shown in Table 6.2, we find that the convergence rates for $(\mathbf{p}_h, u_h, \boldsymbol{\lambda}_h)$ are given by

$$\begin{aligned} \|\mathbf{p} - \mathbf{p}_h\|_0 &\sim \mathcal{O}(h), & \|\boldsymbol{\lambda} - \boldsymbol{\lambda}_h\|_0 &\sim \mathcal{O}(h), \\ \|u - u_h\|_1 &\sim \mathcal{O}(h), & \|u - u_h\|_0 &\sim \mathcal{O}(h^2). \end{aligned}$$

Remember that we are using the piecewise constant finite elements for discretizing \mathbf{p} and $\boldsymbol{\lambda}$, the first-order Lagrange finite elements for discretizing u . This means that expected optimal convergence rates are obtained for all variables.

Table 6.3 shows iteration counts for Newton method with the block preconditioners $\mathcal{B}_h(\mathbf{r})$ and $\tilde{\mathcal{B}}_h(\mathbf{r})$ for different mesh sizes. We see from the relatively consistent iteration counts that both the exact and inexact preconditioners are robust with respect to the mesh size. This demonstrates the optimality of the linear solver and the efficiency of the preconditioners. Compared with using the exact block preconditioners, using the inexact one results in a slight degradation in performance, but nothing significant and negligible.

For comparisons, we present the corresponding results for Picard method in Table 6.4. Observe that the linear iteration numbers of MINRES method for these two methods are almost the same but

TABLE 6.3

Iteration counts for Newton method with the block preconditioners $\mathcal{B}_h(\mathbf{r})$ and $\tilde{\mathcal{B}}_h(\mathbf{r})$ (Example 6.1).

mesh	$\mathcal{B}_h(\mathbf{r})$	$\tilde{\mathcal{B}}_h(\mathbf{r})$
	$N_{\text{Newton}}(N_{\text{MINRES}})$	$N_{\text{Newton}}(N_{\text{MINRES}})$
\mathcal{T}_1	5(21)	5(26)
\mathcal{T}_2	5(20)	5(25)
\mathcal{T}_3	5(20)	5(25)
\mathcal{T}_4	5(19)	5(25)

TABLE 6.4

Iteration counts for Picard method with the block preconditioners $\mathcal{B}_h(\mathbf{r})$ and $\tilde{\mathcal{B}}_h(\mathbf{r})$ (Example 6.1).

mesh	$\mathcal{B}_h(\mathbf{r})$	$\tilde{\mathcal{B}}_h(\mathbf{r})$
	$N_{\text{Picard}}(N_{\text{MINRES}})$	$N_{\text{Picard}}(N_{\text{MINRES}})$
\mathcal{T}_1	36(19)	36(24)
\mathcal{T}_2	33(19)	33(24)
\mathcal{T}_3	30(18)	30(24)
\mathcal{T}_4	26(18)	26(23)

the nonlinear iteration numbers of Newton method are much less than those of Picard method. Using mesh \mathcal{T}_4 , we display the convergence histories of Picard method and Newton method in Figure 6.1. We see that Newton method shows a dramatic faster convergence than the Picard method.

In Table 6.5, we further give the iteration numbers of MINRES at each Newton step for the exact and inexact preconditioners. From the results, we see that the iteration numbers of MINRES is almost invariant with different mesh sizes and iteration numbers. This verifies that our preconditioners are robust with respect to the iterative steps and mesh sizes. Besides, we again observe that the use of the inexact preconditioners has nearly no impact on the needed number of iterations for MINRES. Using the grid \mathcal{T}_4 , we plot the convergence histories of MINRES method at each Newton step in Figure 6.2. It can be seen that the relative residual decrease rapidly as we expected, which indicates our preconditioners are effective.

TABLE 6.5

Number of MINRES iterations with the block preconditioners $\mathcal{B}_h(\mathbf{r})$ and $\tilde{\mathcal{B}}_h(\mathbf{r})$ at each Newton step (Example 6.1).

h	$\mathcal{B}_h(\mathbf{r})$					$\tilde{\mathcal{B}}_h(\mathbf{r})$				
	1	2	3	4	5	1	2	3	4	5
\mathcal{T}_1	15	18	22	24	25	17	23	26	31	33
\mathcal{T}_2	13	18	22	24	25	17	22	26	31	31
\mathcal{T}_3	13	17	20	23	25	18	22	26	30	31
\mathcal{T}_4	13	17	19	22	25	17	22	26	29	31

Finally, we investigate the robustness of the block preconditioners with respect to the parameters α and β . We fix the mesh \mathcal{T}_3 and vary the parameters. The results for Newton method with the exact and inexact preconditioners are shown in Table 6.6-6.7. We can see that the proposed preconditioner

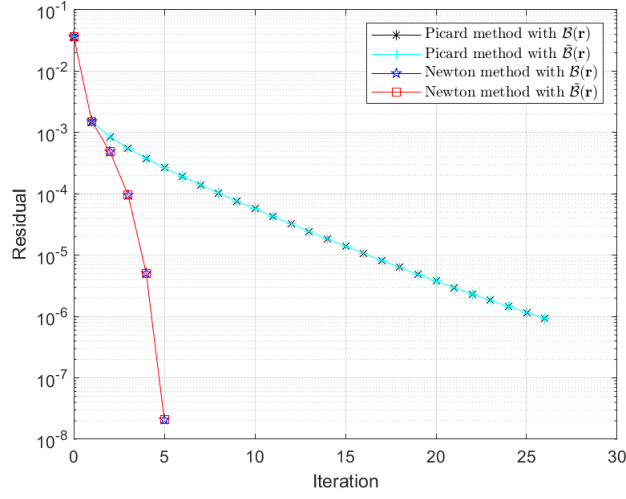


FIG. 6.1. Convergence histories of Picard method and Newton method (Example 6.1).

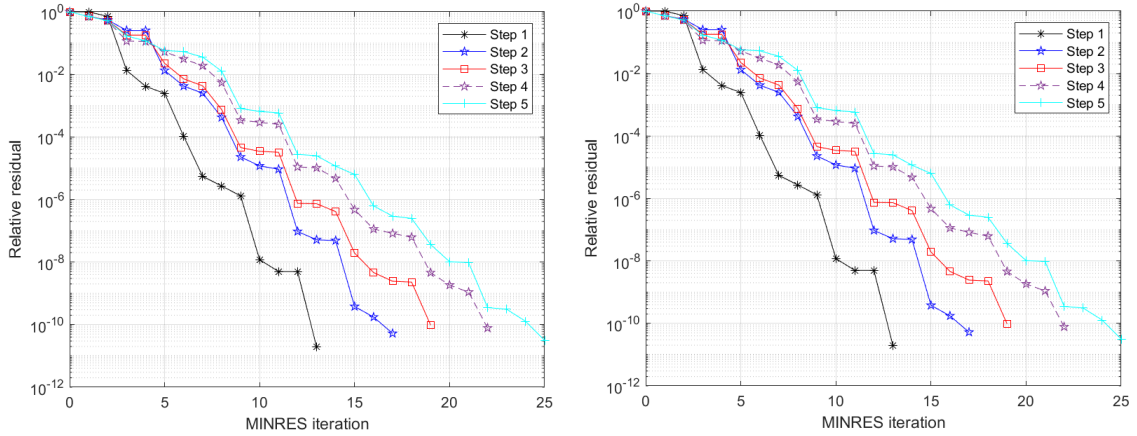


FIG. 6.2. Convergence histories of the preconditioned MINRES method at each Newton step with $\mathcal{B}_h(\mathbf{r})$ (left) and $\tilde{\mathcal{B}}_h(\mathbf{r})$ (right).

are very robust with respect to the parameters, and that the use of the inexact preconditioner has nearly no impact on the required iterations from MINRES.

TABLE 6.6

Iteration counts for Newton method with the block preconditioner $\mathcal{B}_h(\mathbf{r})$ (Example 6.1).

		α				
β	$N_{\text{Newton}}(N_{\text{MINRES}})$	1e5	1e3	1	1e-3	1e-5
	1	7(8)	7(10)	5(20)	2(41)	1(21)
	1e-3	14(10)	13(13)	8(31)	2(28)	2(28)
	1e-5	13(9)	13(10)	10(30)	2(22)	3(29)

TABLE 6.7

Iteration counts for Newton method with the block preconditioner $\tilde{\mathcal{B}}_h(\mathbf{r})$ (Example 6.1).

		α				
β	$N_{\text{Newton}}(N_{\text{MINRES}})$	1e5	1e3	1	1e-3	1e-5
	1	7(12)	7(13)	5(25)	2(41)	1(21)
	1e-3	14(36)	13(33)	8(34)	2(29)	2(28)
	1e-5	13(23)	13(24)	10(34)	2(24)	3(30)

EXAMPLE 6.2. In this example, we consider a non-smooth problem. Let $\Omega = (0, 1)^2$ and denote its center by $x_\Omega := (0.5, 0.5)$. Write $B_r(x_\Omega) = \{x \in \mathbb{R}^2 : \|x - x_\Omega\|_{l_2} < r\}$ with $r = 1/3$, the function f is chosen as a characteristic function $f := \chi_{B_r(x_\Omega)}$. Let I_h be the standard nodal interpolation operator to U_h , the initial guess u_h^0 is taken as $u_h^0 := I_h f$, and (p_h^0, λ_h^0) is computed by the equations (3.1).

First, we aim to investigate the convergence rates. From [27], if $\alpha = 0.02$, the exact solution to the model (1.2) is given by

$$u = \begin{cases} 1 - \frac{2\alpha}{r} = 0.94 & x \in B_r(x_\Omega), \\ \frac{2\pi r \alpha}{1 - \pi r^2} \approx 0.03 & x \in \Omega \setminus B_r(x_\Omega). \end{cases}$$

We perform numerical tests for the primal-dual finite element discretization to (2.2) with $\beta = 1e - 5$. The errors and convergence rates for u are displayed in Table 6.8. Note that the exact solution $u \in L^\infty(\Omega)$, thus the convergence rates are not perfect as the ones in Example 6.1. Even so, the numerical results are in accord with the theoretical results in Proposition 10.9 of [3] for the standard finite element discretization to (1.4). The error estimate of primal-dual finite element discretization is left for further work, we also refer to [9, 10, 11, 19, 31] for some discussions on this direction.

TABLE 6.8

Errors and convergence rates for u_h (Example 6.2).

h	$\ u - u_h\ _0$	Order	$\ u - I_h u\ _0$	Order
6.25e-02	1.12395e-01	—	1.17827e-01	—
3.13e-02	7.94646e-02	0.50	8.35176e-02	0.50
1.56e-02	6.10573e-02	0.38	6.33701e-02	0.40
7.81e-03	4.48697e-02	0.44	4.17839e-02	0.60

In Table 6.9, we present the iteration numbers of Newton method on various meshes. As predicted from the analysis, the numbers of MINRES iterations are stable when we vary the mesh size h . Besides, the iteration numbers for $\tilde{\mathcal{B}}_h(\mathbf{r})$ are only slightly larger than the numbers for $\mathcal{B}_h(\mathbf{r})$. This is expected

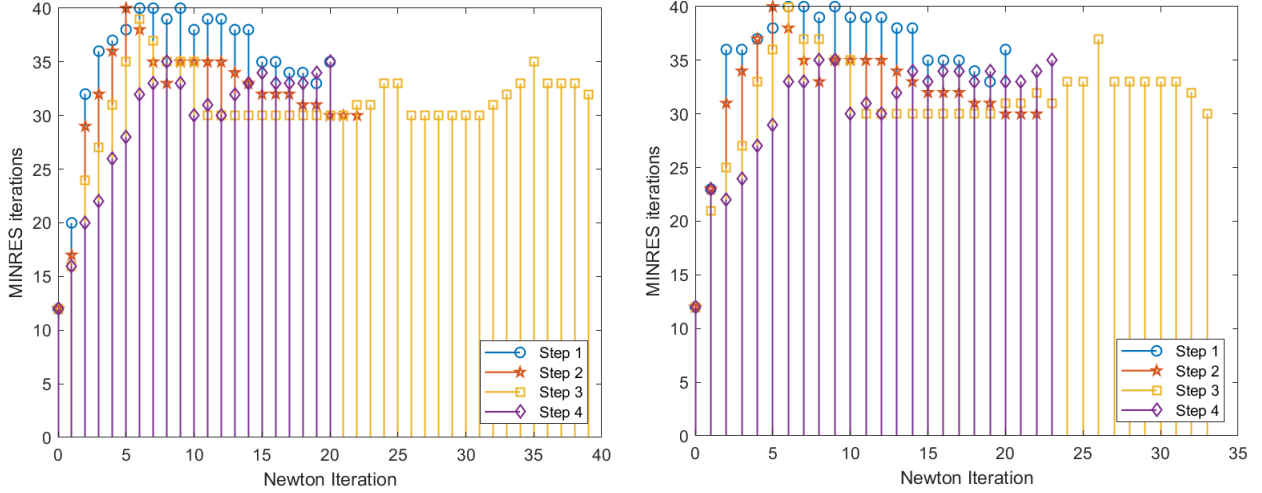


FIG. 6.3. Number of MINRES iterations with the block preconditioners $\mathcal{B}_h(\mathbf{r})$ (left) and $\tilde{\mathcal{B}}_h(\mathbf{r})$ (right) at each Newton step (Example 6.1).

and the difference is by no means significant. Overall, we can conclude that our preconditioners are effective and robust with respect to the mesh size h . Figure 6.3 plots the iteration numbers of MINRES at each Newton step. Again, we observe relative robustness with respect to the iterative step. Specifically, Figure 6.4 shows the damping parameter with respect to the iterative step on mesh \mathcal{T}_4 . We find that the damping strategy is crucial to guarantee the global convergence of Newton's method.

TABLE 6.9

Iteration counts for Newton method with the block preconditioners $\mathcal{B}_h(\mathbf{r})$ and $\tilde{\mathcal{B}}_h(\mathbf{r})$ (Example 6.2).

mesh	$\mathcal{B}_h(\mathbf{r})$	$\tilde{\mathcal{B}}_h(\mathbf{r})$
	$N_{\text{Newton}}(N_{\text{MINRES}})$	$N_{\text{Newton}}(N_{\text{MINRES}})$
\mathcal{T}_1	21(35)	21(35)
\mathcal{T}_2	23(32)	23(32)
\mathcal{T}_3	40(31)	34(31)
\mathcal{T}_4	21(29)	24(31)

As in the previous example, we vary the parameters α and β to study the robustness of the preconditioners. Table 6.10-6.11 show the results for Newton method with the exact and inexact preconditioners on mesh \mathcal{T}_3 . Again, we see that the preconditioners show relative robustness with respect to the parameters. The inexact preconditioner requires a slightly higher number of iterations to converge compared to the exact one, as we saw in the previous example.

For comparison, we present the number of iterations required by Picard method for different α and β on mesh \mathcal{T}_3 in Tables 6.12-6.13. Compared with the results of Newton method, we can see that the Newton iteration converges rapidly than the Picard iteration for the considered parameters. For the case of $\alpha = 1e - 2, \beta = 1e - 3$, Figure 6.5 plots the convergence histories of Picard method and Newton method with $\mathcal{B}_h(\mathbf{r})$ and $\tilde{\mathcal{B}}_h(\mathbf{r})$. As we conclude, the Newton iteration behaves similarly to

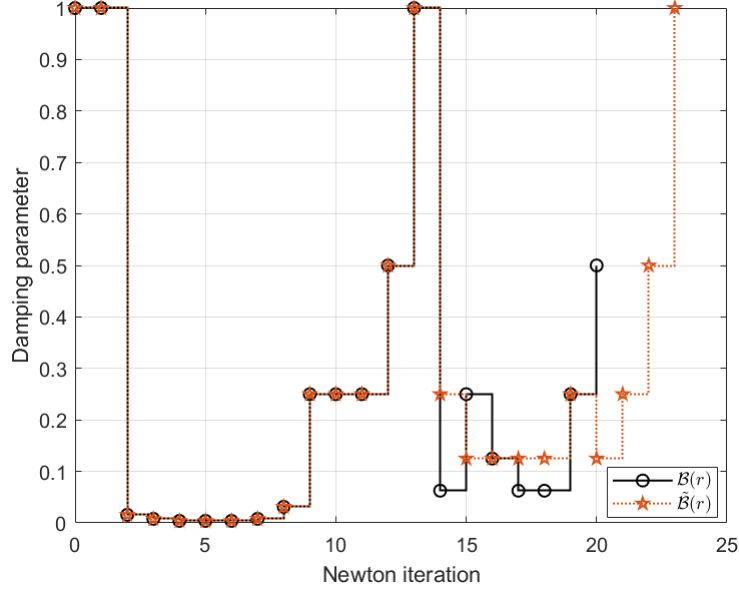


FIG. 6.4. Damping parameter at each Newton iteration with $\mathcal{B}_h(\mathbf{r})$ and $\tilde{\mathcal{B}}_h(\mathbf{r})$ on mesh \mathcal{T}_4 .

TABLE 6.10

Iteration counts for Newton method with the block preconditioner $\mathcal{B}_h(\mathbf{r})$. (Example 6.2)

		α			
β	$N_{\text{Newton}}(N_{\text{MINRES}})$	1e-1	5e-2	1e-2	5e-3
	1	22(28)	8(35)	5(46)	4(49)
	1e-1	31(26)	6(31)	10(43)	9(45)
	1e-2	27(21)	7(28)	9(40)	12(41)
	1e-3	10(18)	8(25)	15(39)	18(37)

TABLE 6.11

Iteration counts for Newton method with the block preconditioner $\tilde{\mathcal{B}}_h(\mathbf{r})$ (Example 6.2).

		α			
β	$N_{\text{Newton}}(N_{\text{MINRES}})$	1e-1	5e-2	1e-2	5e-3
	1	22(33)	8(42)	5(46)	4(49)
	1e-1	31(30)	6(35)	10(44)	9(45)
	1e-2	37(25)	7(30)	9(42)	12(41)
	1e-3	10(22)	8(27)	18(39)	18(37)

the Picard iteration in the early stages but converges rapidly in the end stages.

EXAMPLE 6.3. This example we consider is a benchmark problem as seen in [2, 4, 29]. Let $\Omega = (0, 1)^2$ and denote its center by x_Ω . Given a triangulation \mathcal{T}_h of Ω , we define a randomly perturbed $\xi_h \in U_h$, whose coefficient vector is sampled from the normally distributed. Write $B_r^p(x_\Omega) = \{x \in \mathbb{R}^d : |x - x_\Omega|_{l_p} < r\}$ with $r = 1/3$ and $p \in [1, \infty]$, the function f is set by a characteristic function

TABLE 6.12

Iteration counts for Picard method with the block preconditioner $\mathcal{B}_h(\mathbf{r})$. (Example 6.2)

		α			
β	$N_{\text{Picard}}(N_{\text{MINRES}})$	1e-1	5e-2	1e-2	5e-3
	1	20(27)	26(31)	13(44)	9(50)
	1e-1	39(22)	37(27)	18(37)	12(42)
	1e-2	68(19)	52(24)	23(31)	16(35)
	1e-3	90(18)	71(22)	29(29)	20(32)

TABLE 6.13

Iteration counts for Picard method with the block preconditioner $\tilde{\mathcal{B}}_h(\mathbf{r})$ (Example 6.2).

		α			
β	$N_{\text{Picard}}(N_{\text{MINRES}})$	1e-1	5e-2	1e-2	5e-3
	1	20(33)	26(39)	13(45)	9(50)
	1e-1	39(28)	37(34)	18(42)	12(45)
	1e-2	68(24)	52(31)	23(38)	16(42)
	1e-3	90(22)	71(29)	29(36)	20(39)

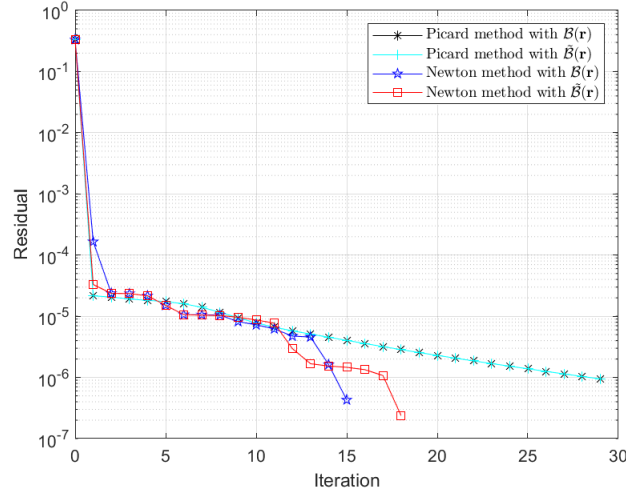


FIG. 6.5. Convergence histories of Picard method and Newton method (Example 6.2).

$f_0 := \chi_{B_r^p(x_\Omega)}$ that is mesh-dependent perturbed ξ_h , precisely,

$$f = f_0 + \delta \xi_h, \quad \text{with } \delta = 0.1.$$

The parameters are given by $\alpha = 5e-2$ and $\beta = 1e-3$. The initial value for Picard method is set as Example 6.2. While for Newton method, the initial value is taken as 5-step iterations of Picard method to improve its efficiency.

To experimentally study the effectiveness of the proposed method, we run Picard method and Newton with $p = 1, 2, \infty$ on mesh \mathcal{T}_4 . Figure 6.6 displays the initial data and the outputs of the iterative schemes. Notice that Newton method and Picard method yield very similar results. From

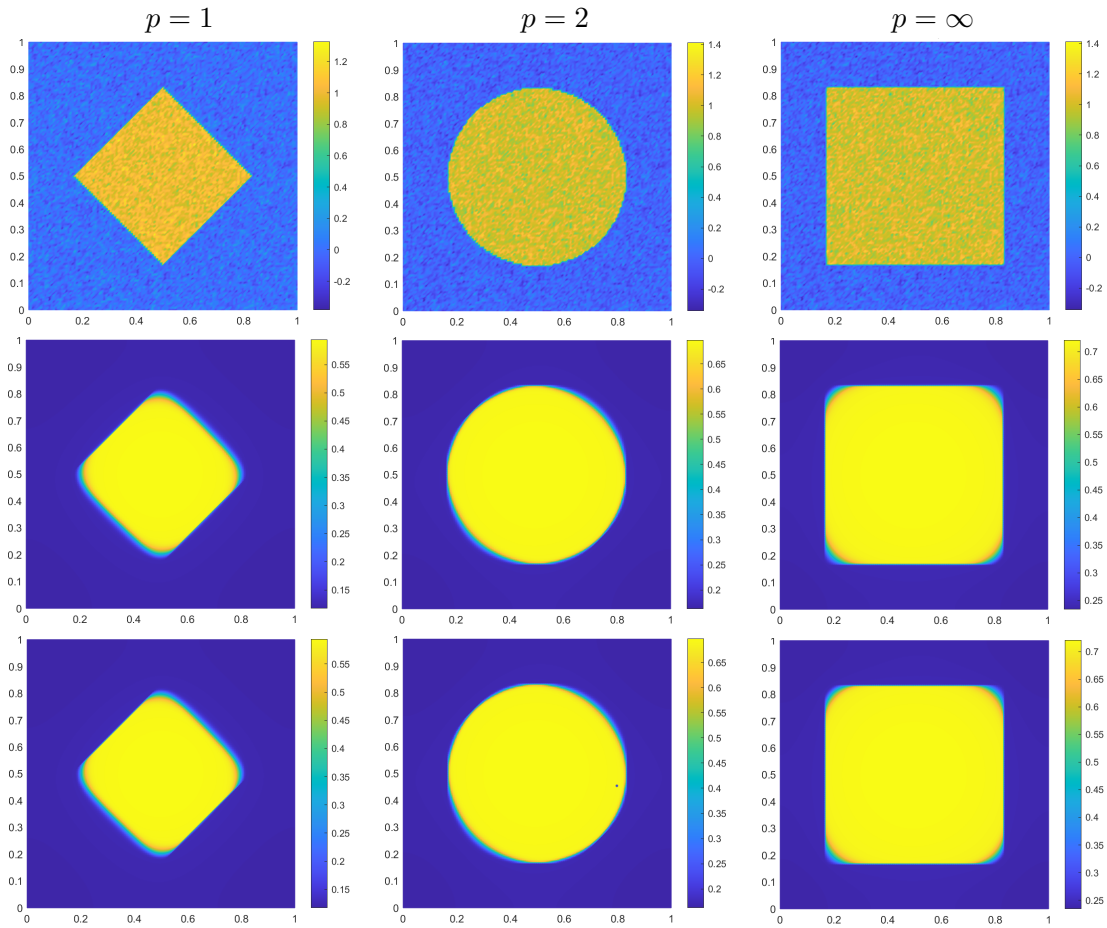


FIG. 6.6. Noisy image, denoised image with Picard method and denoised image with Newton method (from top to bottom).

TABLE 6.14
Iteration counts for Picard method and Newton method (Example 6.3).

p	$N_{\text{Picard}}(N_{\text{MINRES}})$	$N_{\text{Newton}}(N_{\text{MINRES}})$
1	66(29)	16(41)
2	67(30)	19(39)
∞	86(29)	18(43)

the outputs, we see that noise is removed effectively. The boundary is slightly smoothed, especially the corner and the numerical results indeed show the inherited properties of the ROF model.

In Table 6.14, we display the iteration numbers for Picard method and Newton method with $\widetilde{\mathcal{B}}_h(\mathbf{r})$. We again observe that Newton method needs less iteration numbers than Picard method. We further plot the convergence histories of this experiment in Figure 6.7. We see that Newton method converges much faster than Picard method after a few damped Newton updatings.

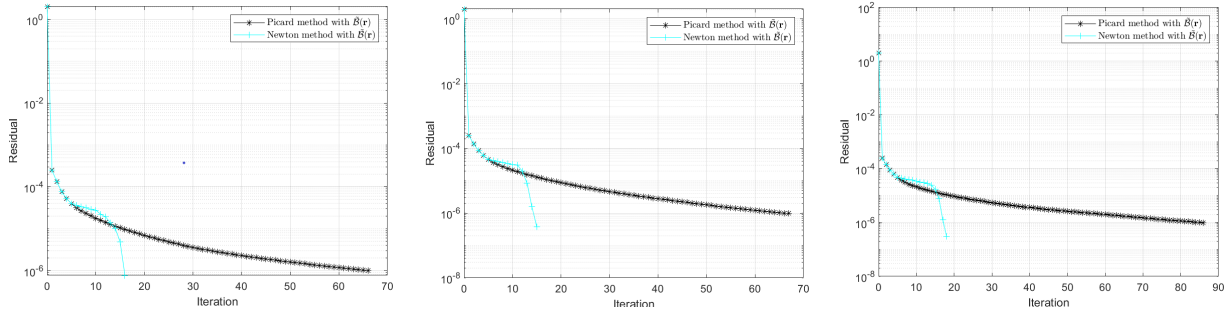


FIG. 6.7. Convergence histories of Picard method and Newton method for $p = 1, 2, \infty$ (from left to right) (Example 6.3).

7. Conclusions. In this paper, we propose a preconditioned Newton solver for primal-dual finite element approximation of total variation minimization and minimum surface problems. We develop some block diagonal preconditioners for the discrete problems at each Newton iteration, which are robust with respect to the mesh size, the penalization parameter, the regularization parameter, and the iterative step. We further prove that the resulting preconditioned MINRES converges uniformly. The theoretical findings are demonstrated by numerical experiments.

REFERENCES

- [1] R. ACAR AND C. R. VOGEL, *Analysis of bounded variation penalty methods for ill-posed problems*, Inverse Problems, 10 (1994), pp. 1217–1229.
- [2] S. BARTELS, *Total variation minimization with finite elements: convergence and iterative solution*, SIAM J. Numer. Anal., 50 (2012), pp. 1162–1180.
- [3] S. BARTELS, *Numerical methods for nonlinear partial differential equations*, vol. 47 of Springer Series in Computational Mathematics, Springer, Cham, 2015.
- [4] S. BARTELS, L. DIENING, AND R. H. NOCHETTO, *Unconditional stability of semi-implicit discretizations of singular flows*, SIAM J. Numer. Anal., 56 (2018), pp. 1896–1914.
- [5] S. BARTELS, R. H. NOCHETTO, AND A. J. SALGADO, *A total variation diminishing interpolation operator and applications*, Math. Comp., 84 (2015), pp. 2569–2587.
- [6] W. L. BRIGGS, V. E. HENSON, AND S. F. MCCORMICK, *A multigrid tutorial*, Society for Industrial and Applied Mathematics (SIAM), Philadelphia, PA, second ed., 2000.
- [7] E. CASAS, K. KUNISCH, AND C. POLA, *Regularization by functions of bounded variation and applications to image enhancement*, Appl. Math. Optim., 40 (1999), pp. 229–257.
- [8] A. CHAMBOLLE, *An algorithm for total variation minimization and applications*, J. Math. Imaging Vision, 20 (2004), pp. 89–97. Special issue on mathematics and image analysis.
- [9] A. CHAMBOLLE, S. E. LEVINE, AND B. J. LUCIER, *An upwind finite-difference method for total variation-based image smoothing*, SIAM J. Imaging Sci., 4 (2011), pp. 277–299.
- [10] A. CHAMBOLLE AND T. POCK, *Crouzeix-Raviart approximation of the total variation on simplicial meshes*, J. Math. Imaging Vision, 62 (2020), pp. 872–899.
- [11] A. CHAMBOLLE AND T. POCK, *Approximating the total variation with finite differences or finite elements*, in Geometric partial differential equations. Part II, vol. 22 of Handb. Numer. Anal., Elsevier/North-Holland, Amsterdam, [2021] ©2021, pp. 383–417.
- [12] T. F. CHAN, G. H. GOLUB, AND P. MULET, *A nonlinear primal-dual method for total variation-based image restoration*, SIAM J. Sci. Comput., 20 (1999), pp. 1964–1977.
- [13] T. F. CHAN AND J. SHEN, *On the role of the BV image model in image restoration*, in Recent advances in scientific computing and partial differential equations (Hong Kong, 2002), vol. 330 of Contemp. Math., Amer. Math. Soc., Providence, RI, 2003, pp. 25–41.

- [14] L. CHEN, *iFEM: an integrated finite element methods package in MATLAB*, Technical Report, University of California at Irvine, (2009).
- [15] D. C. DOBSON AND C. R. VOGEL, *Convergence of an iterative method for total variation denoising*, SIAM J. Numer. Anal., 34 (1997), pp. 1779–1791.
- [16] T. GOLDSTEIN AND S. OSHER, *The split Bregman method for L1-regularized problems*, SIAM J. Imaging Sci., 2 (2009), pp. 323–343.
- [17] W. HACKBUSCH, *Iterative solution of large sparse systems of equations*, vol. 95 of Applied Mathematical Sciences, Springer, [Cham], second ed., 2016.
- [18] Q. HU, X. TAI, AND R. WINTHER, *A saddle point approach to the computation of harmonic maps*, Siam J. Numer. Anal., 47 (2009), pp. 1500–1523.
- [19] M.-J. LAI AND L. MATAMBA MESSI, *Piecewise linear approximation of the continuous Rudin-Osher-Fatemi model for image denoising*, SIAM J. Numer. Anal., 50 (2012), pp. 2446–2466.
- [20] D. LAO AND S. ZHAO, *Fundamental theories and their applications of the calculus of variations*, Springer, Singapore; Beijing Institute of Technology Press, Beijing, 2021.
- [21] C.-O. LEE, E.-H. PARK, AND J. PARK, *A finite element approach for the dual Rudin-Osher-Fatemi model and its nonoverlapping domain decomposition methods*, SIAM J. Sci. Comput., 41 (2019), pp. B205–B228.
- [22] D. LIBERZON, *Calculus of variations and optimal control theory*, Princeton University Press, Princeton, NJ, 2012. A concise introduction.
- [23] K.-A. MARDAL AND R. WINTHER, *Preconditioning discretizations of systems of partial differential equations*, Numer. Linear Algebra Appl., 18 (2011), pp. 1–40.
- [24] A. MARQUINA AND S. OSHER, *Explicit algorithms for a new time dependent model based on level set motion for nonlinear deblurring and noise removal*, SIAM J. Sci. Comput., 22 (2000), pp. 387–405.
- [25] S. OSHER AND R. FEDKIW, *Level set methods and dynamic implicit surfaces*, vol. 153 of Applied Mathematical Sciences, Springer-Verlag, New York, 2003.
- [26] L. I. RUDIN, S. OSHER, AND E. FATEMI, *Nonlinear total variation based noise removal algorithms*, Phys. D, 60 (1992), pp. 259–268. Experimental mathematics: computational issues in nonlinear science (Los Alamos, NM, 1991).
- [27] D. STRONG AND T. CHAN, *Edge-preserving and scale-dependent properties of total variation regularization*, Inverse Problems, 19 (2003), pp. S165–S187. Special section on imaging.
- [28] X.-C. TAI AND C. WU, *Augmented lagrangian method, dual methods and split bregman iteration for rof model*, in Scale Space and Variational Methods in Computer Vision, X.-C. Tai, K. Mørken, M. Lysaker, and K.-A. Lie, eds., Berlin, Heidelberg, 2009, Springer Berlin Heidelberg, pp. 502–513.
- [29] W. TIAN AND X. YUAN, *Convergence analysis of primal-dual based methods for total variation minimization with finite element approximation*, J. Sci. Comput., 76 (2018), pp. 243–274.
- [30] C. R. VOGEL AND M. E. OMAN, *Iterative methods for total variation denoising*, SIAM J. Sci. Comput., 17 (1996), pp. 227–238. Special issue on iterative methods in numerical linear algebra (Breckenridge, CO, 1994).
- [31] J. WANG AND B. J. LUCIER, *Error bounds for finite-difference methods for Rudin-Osher-Fatemi image smoothing*, SIAM J. Numer. Anal., 49 (2011), pp. 845–868.
- [32] C. WU AND X.-C. TAI, *Augmented Lagrangian method, dual methods, and split Bregman iteration for ROF, vectorial TV, and high order models*, SIAM J. Imaging Sci., 3 (2010), pp. 300–339.
- [33] J. XU, X.-C. TAI, AND L.-L. WANG, *A two-level domain decomposition method for image restoration*, Inverse Probl. Imaging, 4 (2010), pp. 523–545.
- [34] J. XU AND L. ZIKATANOV, *Algebraic multigrid methods*, Acta Numer., 26 (2017), pp. 591–721.
- [35] C. H. YAO, *Finite element approximation for TV regularization*, Int. J. Numer. Anal. Model., 5 (2008), pp. 516–526.